Unraveling the Symmetry Effects on the Second-Order Nonlinear Optical Responses of Molecular Switches

Beaujean, Pierre; Champagne, Benoît

Published in:
Inorganic Chemistry

DOI:
10.1021/acs.inorgchem.1c03077

Publication date:
2022

Document Version
Publisher's PDF, also known as Version of record

Inorganic Chemistry

pubs.acs.org/IC

Article

Unraveling the Symmetry Effects on the Second-Order Nonlinear Optical Responses of Molecular Switches: The Case of Ruthenium Complexes

Pierre Beaujean and Benoît Champagne*

Cite This: https://doi.org/10.1021/acs.inorgchem.1c03077

Read Online

ACCESS | Metrics & More | Article Recommendations | Supporting Information

ABSTRACT: Owing to their odd order, second-order nonlinear optical (NLO) responses are very sensitive to symmetry. Therefore, within hyper-Rayleigh scattering (HRS) technique, the symmetry impacts the amplitude of the molecular responses, the HRS first hyperpolarizability (β_{HRS}), and the depolarization ratio (DR). Starting from a challenging octupolar structure bearing six ruthenium(II) ammine centers π-conjugated via quaterpyridyl moieties to a tris-chelated zinc(II) core, together with its Λ shape and one-dimensional analogues built by replacing one or two Ru-quaterpyridyl moieties with bipyridine moieties, (time-dependent) density functional theory calculations have been enacted to unravel the symmetry−NLO response relationships as well as their $Ru^{II/III}$ redox-triggered switching effects. The one-dimensional and Λ-shaped NLOphores present β_{HRS} values ∼3 times larger than those of the octupolar system, for both Ru oxidation states. However, using the few-state valence bond-charge transfer models demonstrates that the β_{HRS} response of the octupolar complex cation can become larger than those of its one-dimensional and Λ-shaped analogues provided stronger donor−acceptor groups are employed. In parallel, the DRs decrease from a strong dipolar character (DR ≈ 6) for the one-dimensional chromophore to a weaker dipolar character (DR ≈ 5) for the Λ-shaped one and to a clear octupolar character (DR ≈ 1.7) for the last one. In all cases, the β responses originate mostly from metal-to-ligand charge transfer excited states, as revealed using a new scheme for analyzing the variations in electron density upon excitation. The $Ru^{II/III}$ oxidations lead to a strong decrease in the β_{HRS} responses, which is attributed to the loss of the donor character of the Ru centers and therefore to the reduction of the push−pull π-conjugation. These results demonstrate that the NLO contrast and the NLO switching behavior of these Ru cations are maintained for the different molecular symmetries. Finally, the character of the β responses of the oxidized species, as revealed by the DR values, further evidences a clear evolution from dipolar to octupolar NLOphores.

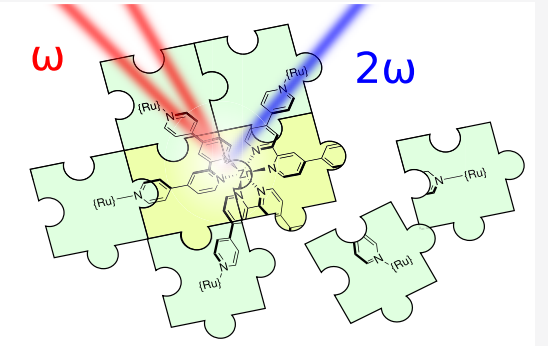

1. INTRODUCTION

For many years, the field of nonlinear optical (NLO) switches has attracted attention for their applications in optoelectronics and photonics.[1−5] The trigger can actually take different forms: light irradiation, pH, or redox potential modifications, recognition of specific analytes, etc. At the molecular level, the central property of these switches is generally the first hyperpolarizability, β. The β characteristics can be probed experimentally by using phenomena and techniques such as hyper-Rayleigh scattering[6−8] (HRS), Stark spectroscopy,[9] and electric-field-induced second harmonic generation (EFISHG).[10,11] In parallel, theoretical tools have been developed to rationalize the results as well as to design new, improved, structures.[11−14]

In the past, many one-dimensional dipolar NLO switches have been studied. To a good approximation, their β response is dictated by one low-excitation energy charge transfer (CT) excited state.[15−20] Among them, ruthenium complexes, which constitute the broadest family of organometallic NLO compounds, were extensively scrutinized by Coe and co-workers,[21] first from an experimental[22−29] point of view, owing to the large first hyperpolarizabilities of the Ru^{II} species. These studies have fostered quantum chemistry investigations[30−37] targeting the interpretation of the NLO response of these Ru-containing compounds, contributing therefore to their design, or aiming at the assessment of their performance (e.g., choice of atomic basis sets, role of electron correlation, and description of frequency dispersion). These large β values have been ascribed to a strong metal-to-ligand charge transfer (MLCT) excited state, which can be altered reversibly through a $Ru^{II/III}$ redox switching. In addition to one-dimensional

Received: October 4, 2021

Scheme 1. Complex Cation 5 and Its Substructures (1−4)[a]

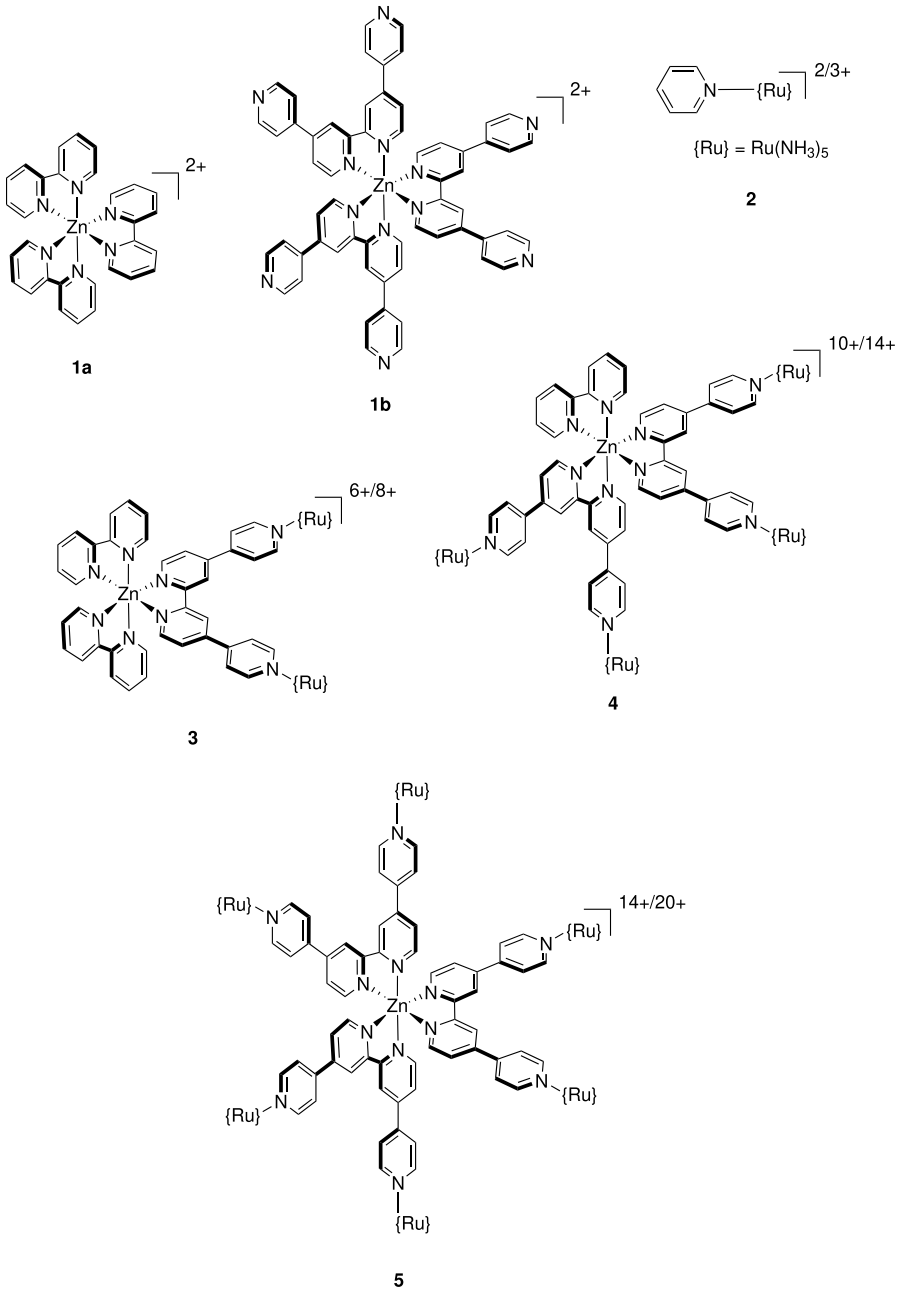

[a]For the structures with Ru atoms, the first (second) charge corresponds to the fully reduced (oxidized) form.

dipolar structures, already 30 years ago, Zyss drew to alternative architectures,[38] such as the octupolar compounds, which can also exhibit large β values, similar to those of their dipolar counterparts. These results were rationalized using theoretical means, e.g., a simple four-state model.[39] Here, challenged by Benjamin J. Coe,[40] we study a rather complex example of such octupolar transition metal NLO switches, complex cation **5** (Scheme 1), which contains six switchable ruthenium centers arranged in a D_3 fashion. This cation bears six ruthenium(II) amine centers π-conjugated via quaterpyridyl moieties to a tris-chelated zinc(II) core. The primary goal is to study, by using well-selected quantum chemistry methods, its first hyperpolarizability, in light of its geometrical and electronic structures and its ultraviolet/visible (UV/vis) absorption properties. To gain such an insight into the structure−property relationships, different substructures of **5** (cations **1**−**4**) are also characterized and, when available, the quantum chemistry results are compared to experimental data. Note that we restrict ourselves to the fully reduced (all Ru atoms are in oxidation state II, noted $\mathbf{x}^{\mathbf{II}}$) or fully oxidized ($\mathbf{x}^{\mathbf{III}}$) cases. A secondary goal is to unravel the relationships between the first hyperpolarizability and the molecular symmetry because, starting from cation **5**, the removal of the Ru units on one arm leads to the push−pull π-conjugated Λ-shaped cation **4**, while the removal of a pair of such units restores a push−pull one-dimensional-like structure (cation **3**). From these analyses, design strategies for enhancing the β contrast are then suggested.

This paper is divided into four parts. After the methodological and computational issues are described in section 2, the

https://doi.org/10.1021/acs.inorgchem.1c03077
Inorg. Chem. XXXX, XXX, XXX−XXX

results (geometrical structures, first hyperpolarizabilities, and their analysis via the few-state approximations) are presented and discussed in section 3. Finally, section 4 summarizes the key results and draws conclusions.

2. METHODOLOGICAL AND COMPUTATIONAL ELEMENTS

2.1. HRS Responses. The focus of this paper is the first hyperpolarizability as it can be measured using the HRS technique.[6−8] The following setup is considered. Within the laboratory frame, the incident light propagates along the Y axis and the Z-polarized scattered light is collected in the X direction. According to the parallel (Z-polarized) and perpendicular (X-polarized) polarization of the incident light, the intensity is proportional to the orientational averages $\langle\beta_{ZZZ}^2\rangle$ and $\langle\beta_{ZXX}^2\rangle$, respectively. Also, for nonpolarized incident light, the square of the molecular β_{HRS} is defined as the sum of those two quantities:

$$\beta_{HRS} = \sqrt{\langle\beta_{ZZZ}^2\rangle + \langle\beta_{ZXX}^2\rangle} \tag{1}$$

while the depolarization ratio

$$DR = \frac{\langle\beta_{ZZZ}^2\rangle}{\langle\beta_{ZXX}^2\rangle} \tag{2}$$

is indicative of the geometry and symmetry of the NLOphore. In the static limit, DR = 1.5 for perfect octupolar compounds while DR = 9 for purely dipolar geometries.[41−43] All reported β values are given in au (1 au of $\beta = 3.6212 \times 10^{-42}$ m^4 V^{-1} = 3.2064×10^{-53} C^3 m^3 J^{-2} = 8.639×10^{-33} esu) within the T convention.[11]

2.2. DFT Molecular Geometries. Full geometry optimizations were performed for each cation using the Gaussian 16 A03 package.[44] To select a reliable level of approximation for the geometry optimization, different combinations of DFT exchange-correlation functionals (XCFs) and basis sets were employed and the results compared to available XRD structures for cation **2** in its reduced and oxidized forms. These structures are referenced in the Cambridge Structural Database[45] as NEFXUR for $\mathbf{2}^{II}$ (reduced form, singlet) and NEFYAY $\mathbf{2}^{III}$ (oxidized form, doublet).[46] Emphasis was placed on the reproduction of the modification of bond lengths (mostly those involving the Ru atom) induced by redox switching. Tables S1 and S2 demonstrate that a triple-ζ basis set is mandatory for the first- and second-row atoms as well as for Ru. This led to selecting the B3P86[47]/6-311G(d)/LANL2TZ[48,49] [and 6-31G(d) for Zn] level and using it to optimize the structure of **1** and the fully reduced and oxidized forms of **3**−**5**. Vibrational frequency calculations were also carried out on the optimized structures at the same level of approximation to check for the absence of imaginary frequencies and confirm that structures are minima on the potential energy surface.

2.3. TDDFT First Hyperpolarizabilities. The level of approximation was also selected for calculating the NLO properties of those cations. These calculations were enacted using the coupled-perturbed Kohn−Sham (CPKS) scheme[50,51] for the static values and the time-dependent DFT scheme[52] for the dynamic ones. The XCF/basis set combination was selected such as to approach, at the CPKS level, reference values obtained at the MP2/cc-pVTZ/LANL2TZ(f)[53] level for both oxidation states of **2**. Note that the MP2 values are evaluated using the finite-field method, corresponding to a numerical differentiation[54−57] of the field-dependent energy, whereas the CPKS and TDDFT values were obtained using a self-consistent analytical derivative scheme. As shown in Table S3, all tested XCFs overestimate the β_{HRS} of the oxidized form. The LC-BLYP[58]/6-311G(d)/LANL2TZ [with 6-31G(d) for Zn] level was chosen because it provides a correct description of the β value of $\mathbf{2}^{II}$, though it underestimates the $\mathbf{2}^{II}/\mathbf{2}^{III}$ ratio. All CPKS/TDDFT calculations were performed in the static limit as well as at typical wavelengths (1907 and 1064 nm). They were performed using Gaussian 16. The molecules are modeled in an acetonitrile solution (ε_0 = 35.688, and ε_∞ = 1.806874), and the effects of these surroundings are simulated within the IEF-PCM implicit solvent formalism.[59−61]

2.4. TDDFT Excitation Energies and Electron Density Reorganization. To rationalize the first hyperpolarizabilities, the first 100 excited states were computed using Gaussian 16 at the same level of approximation as the first hyperpolarizabilities. Note that the LC-BLYP is known to overestimate the transition energies of Ru derivatives with respect to experiment,[34,35] but the trends are correct when this choice allows a consistent treatment of both linear and nonlinear optical responses. Note that those cations present inherent difficulties for quantum chemistry treatments. First, the presence of Ru atoms can imply a low-energy state partially described by doubly excited configuration state functions, which would require a multireference treatment, while the large size of **5** currently prevents this kind of approach. Nevertheless, on this topic, Escudero et al.[37] compared standard TDDFT to DFT/MRCI and ADC(2) and concluded that DFT was suitable for recovering correct trends. For the dominant (large oscillator strength) excited states, the electron densities evaluated ensuring a non-equilibrium solvation model were used to determine the difference between the ground (GS) and excited state (ES) densities at position $\mathbf{r} = (x, y, z)$ in Cartesian coordinates or (r, θ, ϕ) in spherical coordinates:

$$\delta\rho(\mathbf{r}) = \rho^{ES}(\mathbf{r}) - \rho^{GS}(\mathbf{r}) = \rho^{+}(\mathbf{r}) - \rho^{-}(\mathbf{r}) \tag{3}$$

where, following Jacquemin et al.,[62] one has partitioned the excitation-induced electron density difference into its positive

$$\rho^{+}(\mathbf{r}) = \begin{cases} \delta\rho(\mathbf{r}) & \text{if } \delta\rho(\mathbf{r}) > 0 \\ 0 & \text{otherwise} \end{cases} \tag{4}$$

and negative [$\rho^{-}(\mathbf{r}) = \delta\rho(\mathbf{r})$ if $\delta\rho(\mathbf{r}) < 0$] parts, so that the amount of charge transfer is estimated as

$$q_{CT} = \int d\mathbf{r}\rho^{+}(\mathbf{r}) = -\int d\mathbf{r}\rho^{-}(\mathbf{r}) \tag{5}$$

while the charge transfer distance is given by

$$d_{CT} = |\langle\mathbf{r}\rangle^{-} - \langle\mathbf{r}\rangle^{+}|, \text{ where } \langle\mathbf{r}\rangle^{\pm} = \pm\frac{1}{q_{CT}}\int d\mathbf{r}\,\mathbf{r}\,\rho^{\pm}(\mathbf{r}) \tag{6}$$

Owing to the shape of the compounds, in agreement with related developments,[63,64] it was advantageous to use an alternative approach and to represent the radial distribution of this excitation-induced electron difference around a given center (generally the origin of the axes if properly defined according to group theory). The corresponding positive/negative radial electron distributions $\rho_r^{\pm}(r)$ are then defined, within spherical coordinates, as

$$\rho_r^{\pm}(r) = \frac{d\rho^{\pm}(\mathbf{r})}{dr} = \int_0^{2\pi} d\phi \int_0^{\pi} d\theta\, \rho^{\pm}(r, \theta, \phi)\, r^2 \sin\theta \tag{7}$$

Similar to the case for q_{CT}, the amount of radial charge transfer reads

$$q_{r,CT} = \pm\int dr\rho_r^{\pm}(r) \tag{8}$$

while, in parallel to d_{CT}, a charge transfer radius, r_{CT}, reads

$$r_{CT} = \langle r\rangle^{+} - \langle r\rangle^{-}, \text{ where } \langle r\rangle^{\pm} = \pm\frac{1}{q_{r,CT}}\int dr\, r\, \rho_r^{\pm}(r) \tag{9}$$

which represents the radial charge transfer distance. Analysis of the $\rho_r^{\pm}(r)$ graphs helps to determine how each (group of) atom contributes to the change in electron density: $\rho_r(r) = \rho_r^{+}(r) - \rho_r^{-}(r)$ is representative of the electronic reorganization along the transition. Note that the sign of r_{CT} now indicates, upon excitation, whether the electron density moves from the center to the periphery of the structure ($r_{CT} > 0$) or the opposite.

The `cubegen` utility (with the default options) of Gaussian 16 was used to extract the densities. To gather the charge transfer properties, eqs 7−9 were numerically integrated with a homemade code, by linear interpolation of the density with Δr = 0.05 Å and $\Delta\theta = \Delta\phi = \pi/20$.

https://doi.org/10.1021/acs.inorgchem.1c03077
Inorg. Chem. XXXX, XXX, XXX−XXX

2.5. Valence Bond-Charge Transfer Models. Owing to the shape diversity when going from cation **5** to its fragments, successive valence bond *n* charge transfer (VB-*n*CT) state models were applied. They are adequate for providing qualitative insights when discussing structures with multiple donor moieties, like complex cations **3**−**5**. Those molecules are described by one covalent (VB) and *n* charge transfer states: *n* = 1 for cation **3**, *n* = 2 for cation **4**, and *n* = 3 for cation **5** (Scheme 2).[39,65] These models employ effective Hamiltonians to predict the eigenstates (ground and excited states) and their eigenvalues, and therefore the excitation energies, transition dipoles, and state dipoles so that the first hyperpolarizabilitiy can be modeled as a function of the 3 + 1 parameters: the transfer integrals (*t* for VB-CT and *T* for CT-CT) and the mixing coefficient (m_{CT}) between the VB and CT states, which is clamped between −1 and 1 and describes the amount of CT character of each (ground or excited) state, as introduced by Barzoukas, Blanchard-Desce, and co-workers.[18,19,66] For the ground state, an m_{CT} value close to −1 (1) means that it is dominated by the VB (CT) state. m_{CT} = 0 for an equal mixing of the CT and VB states, the so-called cyanine limit.

Scheme 2. Representation of the Successive VB-*n*CT Models (adapted from ref 67, with charge transfer integrals *t* and *T*)

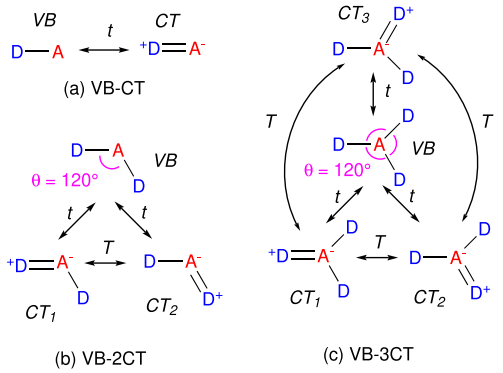

Those VB-*n*CT models were combined with the sum-over-states expression of Orr and Ward,[68] to determine the different components of the β tensor as a function of the shape of the compound. To do so, a last parameter is required, the charge transfer dipole moment, μ_{CT}, which by definition is proportional to the product of the charge of the donor and acceptor (q_{CT}) and the distance (d_{CT}).

2.6. Spin Multiplicity Issues. The oxidized forms are spin multiplets so that the expected exact $\langle S^2 \rangle$ values should be equal to 0.75 ($\mathbf{2}^{III}$, doublet), 2 ($\mathbf{3}^{III}$, triplet), 6 ($\mathbf{4}^{III}$, quintuplet), and 12 ($\mathbf{5}^{III}$, heptuplet). TDDFT excited states are known to exhibit spin contamination when starting from an open-shell ground state.[69] For these multiplets, following Casida and co-workers,[69,70] the $\Delta\langle \hat{S}^2 \rangle = \langle \hat{S}^2 \rangle_e - \langle \hat{S}^2 \rangle_g$ value was also reported for each relevant excited state e, to estimate the spin contamination of the corresponding excited state. Moreover, spin contaminations were monitored for the ground and excited states. Note that the spin densities reveal that the excess of electrons is located only on the Ru atoms.

3. RESULTS AND DISCUSSION

3.1. Geometrical Parameters. To begin, the impact of oxidation on the geometrical parameters is discussed in two steps: the impact on the "core" part of the molecules [around the central Zn atom (Figure 1a)] and then that on the "ruthenium" part (Figure 1b). The different quantities are reported in Table 1, in which they are averaged over the different moieties (e.g., the six Ru centers). A standard deviation is also reported.

Table 1. Impact of Oxidation on the Average Geometrical Parameters Defined in Figure 1 (bond lengths *d* in angstroms and angles *a* in degrees and their standard deviations) Obtained by the Geometry Optimization of 1 and 3−5 at the IEF-PCM(acetonitrile)/B3P86/6-311G(d)/LANL2TZ Level[a]

	1a	1b	2	3	4	5
			$\mathbf{x}^{II}$			
$a_{N[Py(II)]-Zn-N[Py(II)]}$	–	–	–	75.7	75.9 ± 0.0	75.8 ± 0.0
$a_{N[Py(I)]-Zn-N[Py(I)]}$	76.4 ± 0.0	76.2 ± 0.0	–	76.6 ± 0.0	76.5	–
$d_{Zn-N[Py(II)]}$	–	–	–	2.160 ± 0.002	2.157 ± 0.005	2.159 ± 0.004
$d_{Zn-N[Py(I)]}$	2.155 ± 0.000	2.154 ± 0.002	–	2.151 ± 0.002	2.153 ± 0.005	–
$d_{Ru-N[Py(II)]}$	–	–	2.083	2.071 ± 0.001	2.070 ± 0.001	2.070 ± 0.001
$d_{Ru-N(ax)}$	–	–	2.165	2.164 ± 0.000	2.163 ± 0.001	2.163 ± 0.001
t_{bipy}	–	37.1 ± 0.5	–	34.7 ± 0.5	32.1 ± 3.1	32.9 ± 2.7
			$\mathbf{x}^{III}$			
$a_{N[Py(II)]-Zn-N[Py(II)]}$	–	–	–	75.1	75.6 ± 0.0	75.7 ± 0.0
$a_{N[Py(I)]-Zn-N[Py(I)]}$	–	–	–	76.8 ± 0.0	76.9	–
$d_{Zn-N[Py(II)]}$	–	–	–	2.177 ± 0.001	2.166 ± 0.007	2.166 ± 0.004
$d_{Zn-N(I)}$	–	–	–	2.144 ± 0.002	2.145 ± 0.003	–
$d_{Ru-N[Py(II)]}$	–	–	2.100	2.107 ± 0.001	2.110 ± 0.002	2.116 ± 0.002
$d_{Ru-N(ax)}$	–	–	2.142	2.138 ± 0.001	2.134 ± 0.001	2.136 ± 0.002
t_{bipy}	–	–	–	38.2 ± 1.6	38.0 ± 0.5	41.5 ± 3.1
			$\Delta(\mathbf{x}^{III} - \mathbf{x}^{II})$			
$a_{N[Py(II)]-Zn-N[Py(II)]}$	–	–	–	−0.7	−0.4	−0.1
$a_{N[Py(I)]-Zn-N[Py(I)]}$	–	–	–	0.3	0.4	–
$d_{Zn-N[Py(II)]}$	–	–	–	0.017	0.009	0.007
$d_{Zn-N[Py(I)]}$	–	–	–	−0.006	−0.009	0.000
$d_{Ru-N[Py(II)]}$	–	–	0.017	0.036	0.040	0.046
$d_{Ru-N(ax)}$	–	–	−0.023	−0.026	−0.029	−0.027
t_{bipy}	–	–	–	3.4	5.9	8.6

[a]A distinction is made between the bipyridine bearing Ru-bearing moieties [Py(II)] and those without [Py(I)].

https://doi.org/10.1021/acs.inorgchem.1c03077
Inorg. Chem. XXXX, XXX, XXX−XXX

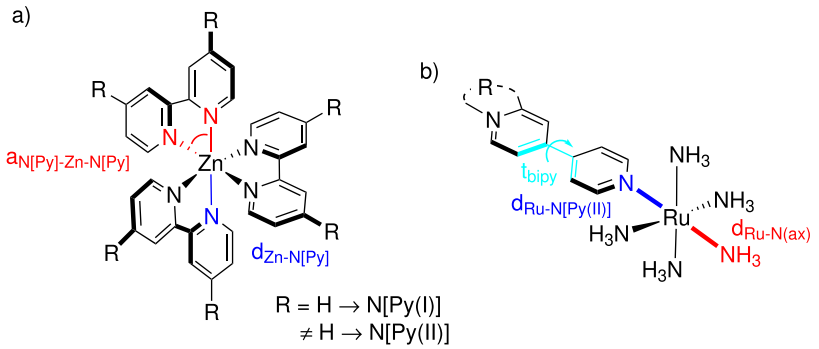

Figure 1. Definition of the geometrical parameters for the (a) "core" part and (b) "ruthenium" part. A distinction is made between the bipyridine bearing Ru-donating moieties [Py(II)] and those without [Py(I)]. "bipy" stands for bipyridine.

Table 2. Static and Dynamic (1907 and 1064 nm) First Hyperpolarizabilities (β_{HRS}, au) of x (x = 1−5) Together with the Ratios between the Two Oxidation States (x^{II}/x^{III}), as Computed at the LC-BLYP/6-311G(d)/LANL2TZ Level in Acetonitrile (IEF-PCM)[a]

	reduced (x^{II})			oxidized (x^{III})			x^{II}/x^{III}		
	static	1907 nm	1064 nm	static	1907 nm	1064 nm	static	1907 nm	1064 nm
1a	83 (1.50)	42 (1.50)	49 (1.50)	–	–	–	–	–	–
1b	57 (1.50)	7 (1.65)	14 (1.46)	–	–	–	–	–	–
2	652 (4.65)	475 (4.67)	612 (4.74)	128 (3.04)	159 (4.02)	192 (4.21)	5.08	2.99	3.19
3	3070 (6.08)	2875 (5.93)	4194 (5.98)	251 (4.49)	837 (6.01)	1055 (6.34)	12.25	3.44	3.98
4	3164 (5.10)	3035 (4.67)	4359 (4.81)	210 (3.03)	682 (3.81)	917 (3.90)	15.13	4.45	4.76
5	986 (1.72)	934 (1.72)	1478 (1.79)	354 (2.92)	343 (1.54)	436 (1.54)	2.79	2.73	3.39

[a]The depolarization ratio (DR) is given in parentheses.

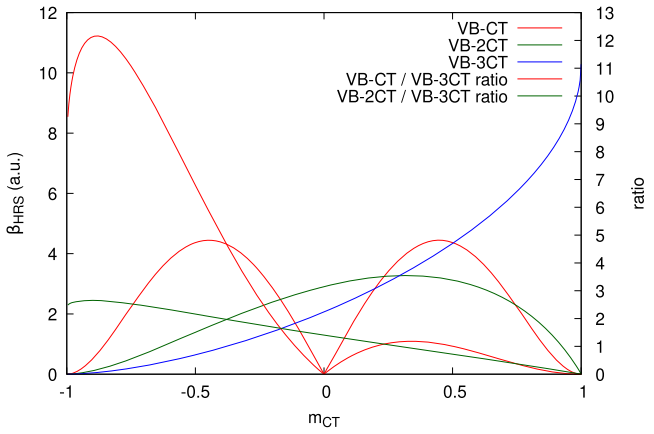

Figure 2. Evolution of β_{HRS} (au) as a function of the CT mixing parameter (m_{CT}) for the three models (thick lines, obtained with $t = T = 0.1\ E_h$ and $\mu_{CT} = 1ea_0$) as well as their ratios (dashed lines).

On one hand, for the "core" part, the presence of Ru-donating moieties (**1a** → **3**, **4**, or **5**) and of oxidation ($x^{II} \rightarrow x^{III}$) both led to a slight decrease in the N[Py(II)]−Zn−N[Py(II)] angles and an increase in the Zn−N[Py(II)] bond lengths. Overall, this part of the molecule remains mostly unaffected because the oxidation effects are localized on the Ru moiety. On the other hand, for the "ruthenium" moieties, the modifications are 1 order of magnitude larger. Again, the presence of the Ru-containing ligands and the oxidation impact the geometry in the same way, though the later is more important. The Ru−N[Py(II)] bond (dark blue in Figure 1b) lengths increase, while the Ru−N(ax) bond (red in Figure 1b) lengths decrease. Both effects are consistent with the weakening, upon oxidation, of the back bonding between the Ru atoms and the pyridyl ligands. An additional clue comes from the modification of the torsion angle between the pyridine rings, which increases upon oxidation. These oxidation-induced modifications are consistent with the observation of Zhang et al.,[34] although more important due to the multiple Ru centers. In conclusion, the effect of oxidation is the reduction of the π-conjugation between the Ru and Zn moieties.

3.2. First Hyperpolarizabilities. The static and dynamic (1907 and 1064 nm) first hyperpolarizabilities of all cations are listed in Table 2. The ordering of the β_{HRS} amplitudes of the reduced forms follows the order

$$\mathbf{1b} < \mathbf{1a} \ll \mathbf{2}^{II} < \mathbf{5}^{II} \ll \mathbf{3}^{II} \approx \mathbf{4}^{II}$$

at the three considered wavelengths. Going from cation **1a** to **3**, i.e., upon addition of a pair of Ru-based donor moieties, results in a huge enhancement of the first hyperpolarizability. Then, adding a second pair increases only slightly β_{HRS}, while it decreases upon the inclusion of a third pair so that the β value becomes comparable to that of cation **2**. The depolarization ratios are close to 5−6 for cations **2**−**4** and close to 1.7 for cations **1** and **5**, evidencing the octupolar character of β associated with the D_3-like symmetry. The DR of cation **3** is actually the largest, corresponding to the most pronounced dipolar character. Moreover, the dynamic β_{HRS} responses of cations **1** and **2** are smaller than the static ones, a fact that originates from a dynamic permittivity of acetonitrile that is smaller than its static counterpart.

After oxidation, β_{HRS} decreases but the trend among the different Ru-containing cations remains

$$\mathbf{2}^{III} < \mathbf{5}^{III} < \mathbf{4}^{III} \approx \mathbf{3}^{III}$$

https://doi.org/10.1021/acs.inorgchem.1c03077
Inorg. Chem. XXXX, XXX, XXX−XXX

Table 3. Nature of the Main Electron Transitions (vertical excitation energy and oscillator strength in parentheses) and Electron Density Difference (negative in blue, isovalue of 0.001 au, two orientations) Together with the Related Quantities [charge transfer amplitude (q_{CT}), distance (d_{CT}), and radius (r_{CT})] of 1a and 1b as Computed at the LC-BLYP/6-311G(d)/LANL2TZ Level in Acetonitrile (IEF-PCM)[a]

1a	1b
ES #1, 258 nm (0.234)	ES #1, 264 nm (0.274)
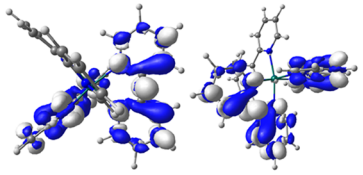	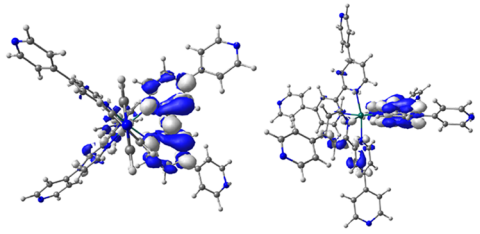
$q_{CT} = 0.43\,e$, $d_{CT} = 0.17$ Å $r_{CT} = -0.09$ Å	$q_{CT} = 0.45\,e$, $d_{CT} = 0.02$ Å $r_{CT} = 0.38$ Å
ES #2, 258 nm (0.241)	ES #2, 264 nm (0.264)
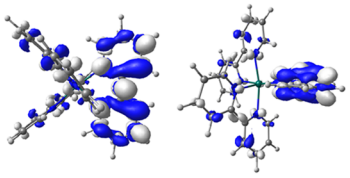	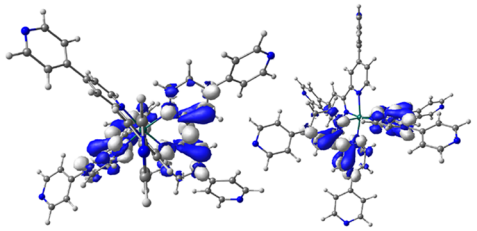
$q_{CT} = 0.42\,e$, $d_{CT} = 0.18$ Å $r_{CT} = -0.13$ Å	$q_{CT} = 0.46\,e$, $d_{CT} = 0.01$ Å $r_{CT} = 0.30$ Å
ES #3, 255 nm (0.779)	ES #3, 261 nm (0.790)
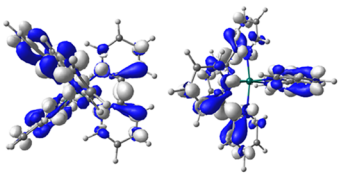	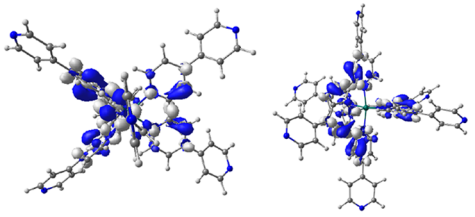
$q_{CT} = 0.40\,e$, $d_{CT} = 0.01$ Å $r_{CT} = -0.09$ Å	$q_{CT} = 0.49\,e$, $d_{CT} = 0.01$ Å $r_{CT} = 0.34$ Å

[a]Two molecular orientations are proposed for each transition state.

except in the static limit, where $\mathbf{3}^{\mathbf{III}} < \mathbf{5}^{\mathbf{III}}$. This inversion is related to frequency dispersion. Therefore, in the dynamic regime, the $\beta_{HRS}(\mathbf{x}^{\mathbf{II}})/\beta_{HRS}(\mathbf{x}^{\mathbf{III}})$ contrast between the two oxidation states is slightly larger than 3 and follows the order

$$\mathbf{2} \approx \mathbf{5} < \mathbf{3} < \mathbf{4}$$

Those ratios are comparable to that reported by Zhang et al.[34] for one-dimensional-like derivatives of cation **2**.

In addition to these fully oxidized (Ru^{III}) and fully reduced (Ru^{II}) states, there are in principal intermediate redox states (e.g., 1, 2, ..., Ru sites of **5** are oxidized) and their linear and nonlinear optical properties might also be distinguishable. However, as observed in previous studies of related compounds,[21,27,28,71] the coupling between the ruthenium units is negligible so that only one oxidation wave is experimentally observed. Therefore, only a short investigation was conducted on cation **5** with total charge of +16 (formally four Ru^{II} and two Ru^{III} atoms) and +18 (formally two Ru^{II} and four Ru^{III} atoms). Calculations performed at the same level of approximation as for the other species demonstrate that partial oxidation or reduction leads to a β_{HRS} response of ~3500 au at 1907 nm with a DR of ~4.0. To a certain extent, this result could have been expected because the partial oxidation or reduction leads to an effective Λ-shaped NLOphore.

3.3. Insights from the VB-*n*CT Models. The first hyperpolarizability of the reduced forms, which are large and dominated by CT transitions, can be analyzed using simple VB-*n*CT models. The evolution of the static β_{HRS} with the CT character (m_{CT}) given in Figure 2 shows variations as a function of the shape. (i) In the simple D/A case, β_{HRS} presents two maxima at $m_{CT} = \pm\sqrt{5}/5 \approx \pm 0.45$.[18,19] (ii) In the VB-2CT model, where $\theta = 120°$ (which corresponds to the angle between the CT dipoles of cation **4**), it exhibits only one maximum located in the $m_{CT} \approx 0.3$ area.[65] (iii) For the VB-3CT model with a D_3-like structure, β_{HRS} increases monotonically with m_{CT}.[38,39] Therefore, (i) D/A pairs of moderate strength favor large β_{HRS} responses with one bridging ligand (featuring the linkers with two Ru atoms), (ii) stronger D/A pairs lead to large responses for structures with two or three bridging ligands, and, finally, (iii) the octupolar species has the

https://doi.org/10.1021/acs.inorgchem.1c03077
Inorg. Chem. XXXX, XXX, XXX−XXX

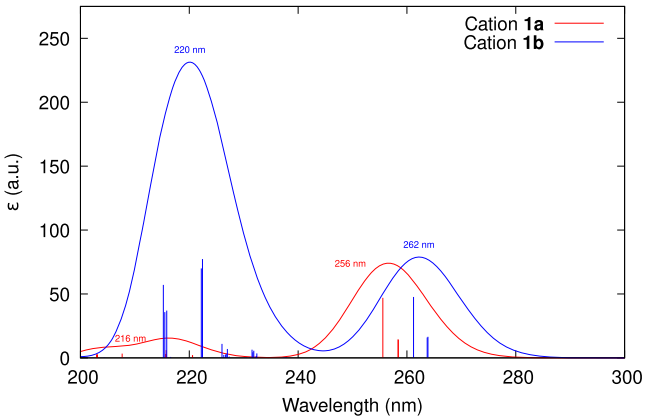

Figure 3. Simulated UV/vis absorption spectra of cations **1a** and **1b**, as computed at the LC-BLYP/6-311G(d)/LANL2TZ level in acetonitrile (IEF-PCM). Each transition is represented by a Gaussian function (full width at half-maximum of 0.3 eV), together with its impulse, which is proportional to the oscillator strength. The different maxima of the curves are also reported.

largest response in the limit of a very large m_{CT}. Assuming that the VB-*n*CT parameters can be considered similar between the compounds, these models help to rationalize the differences in β_{HRS} among cations $\mathbf{3}^{II}$–$\mathbf{5}^{II}$, which are governed by the symmetry. Upon comparison of the relative β_{HRS} amplitudes of $\mathbf{3}^{II}$–$\mathbf{5}^{II}$, it is deduced that $m_{CT} \sim -0.1$, which is not far from the cyanine limit.

On the basis of this analysis, two design strategies for enhancing β are therefore suggested. The simplest consists of increasing m_{CT} (by modification of the donor/acceptor pair), which will increase the β of the octupolar architecture with respect to those of the others. Another, indirect, issue consists of lengthening the π-conjugation path. While this leads to a decrease in m_{CT},[66] it comes together with an increase in the CT dipole moment, which globally leads to an enhancement of β_{HRS}, even though an appropriate balance between the two effects needs to be found. In such a case, the one-dimensional and Λ-shaped structures would present responses larger than those of their octupolar analogues. This strategy was explored by Zhang and Champagne in ref 35 for the reduced forms, resulting in a 4-fold increase in β_{HRS} for derivatives of cation **2**, when increasing the length of the polyenic segment between the pyridine and pyridinium rings.

3.4. Excited States. Figure 3 displays the simulated absorption spectra of cations **1a** and **1b**. To confirm the predictions of the VB-*n*CT models, the important excited states are analyzed and their characteristics are detailed in Table 3. The spectrum presents a first absorption band around 260 nm. Going from **1a** to **1b** slightly increases both the wavelength and the oscillator strength of this band, which is associated with the lengthening of the π-conjugated path. A second, more intense, band around 220 nm appears for cation **1b**. Both are ILCT (intraligand charge transfer) $\pi \rightarrow \pi^*$ transitions that do not involve the Zn atom. This first absorption band is composed of 2 (#1 and #2, located on two ligands) + 1 (#3, located on the three ligands and having the largest intensity) electronic transitions. As expected for the ILCT transition, the charge transfer distances (d_{CT}) are quite small for all three, with a moderate (0.4 *e*) amplitude of the transferred charge. The radial charge densities are similar for all three first excited states of **1a** and **1b** (Figure S1). A representative example (ES #3) is given in Figure 4. For the zone below r = 6 Å, the shapes for **1a** and **1b** are similar: the

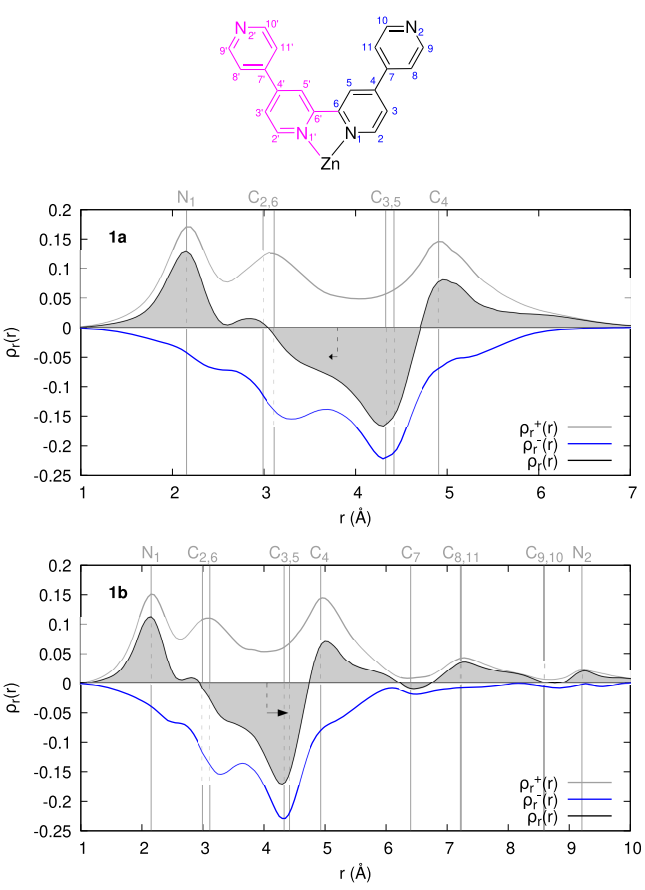

Figure 4. Radial distribution of the electron density difference (centered on the Zn atom) of ES #3 of **1a** (middle, numbering of the atoms on top; the purple atoms are equivalent by symmetry) and **1b** (bottom) as computed at the LC-BLYP/6-311G(d)/LANL2TZ level in acetonitrile (IEF-PCM). The (small) black arrow represents $r_{CT} = \langle r \rangle^+ - \langle r \rangle^-$.

electron density moves mostly from C_3 and C_5 to N_1 and C_4. The peak around 3 Å in ρ_r^+ is due to an increase in the density in the π orbital between C_6 and $C_{6'}$. When $r > 6$ Å, while $\rho_r^{\pm}(r)$ tends toward 0 for **1a**, the second ring also slightly contributes for **1b**. This results in (i) larger r_{CT} values for **1b** than for **1a** (around −0.1 Å for **1a** and 0.3 Å for **1b**) and (ii) a change in the sign, i.e., of direction.

Figure 5 displays the simulated absorption spectrum of both forms of **2**, while Table 4 details the main transitions. The singlet reduced form ($\mathbf{2}^{II}$) displays two important bands, located around 250 and 200 nm, with large q_{CT}, d_{CT}, and $|r_{CT}|$ values. Upon oxidation ($\mathbf{2}^{III}$, doublet), the first excitation band disappears, while two ES appear around 230 nm. The topology of the electron density differences changes and is accompanied by a decrease in the oscillator strength (together with a decrease in q_{CT} and d_{CT}). Note that the spin contamination remains moderate ($0.15 < \Delta\langle S^2 \rangle < 0.4$).

The radial distributions of the electron density difference are plotted in Figure 6 for these excited states. The two transitions in $\mathbf{2}^{II}$ have a similar shape, describing mostly a displacement of the electron density from the Ru atom to the pyridine ring [positive $\rho_r(r)$ when $r < 4$ Å, especially around N_1]. This corresponds to a MLCT transition. On the contrary, $\rho_r(r)$

https://doi.org/10.1021/acs.inorgchem.1c03077
Inorg. Chem. XXXX, XXX, XXX−XXX

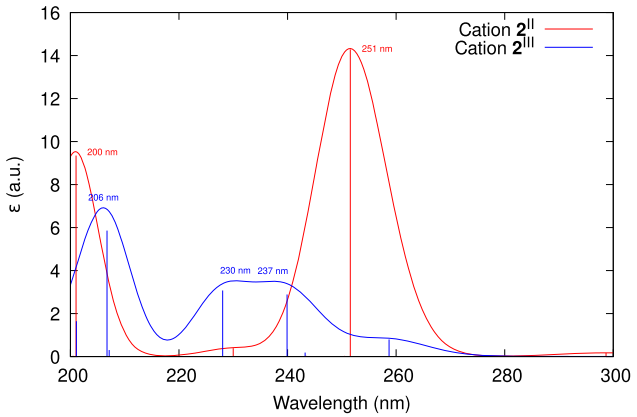

Figure 5. Simulated UV/vis absorption spectra of cations $\mathbf{2}^{II}$ and $\mathbf{2}^{III}$, as computed at the LC-BLYP/6-311G(d)/LANL2TZ level in acetonitrile (IEF-PCM). Each transition is represented by a Gaussian function (full width at half-maximum of 0.3 eV), together with its impulse. The different maxima of the curves are also reported.

shows the opposite trend for ES #1 and #3 of $\mathbf{2}^{III}$. ES #2 of $\mathbf{2}^{III}$ is mostly located on the Ru center, which corresponds to a metal-centered (MC) excited state. It is also noticeable that r_{CT} is positive for $\mathbf{2}^{III}$, which indicates a change in the direction of the electron density displacement upon excitation with respect to the reduced form.

Overall, the important excited states of **1a** and **1b** are ILCT within the pyridine rings. In $\mathbf{2}^{II}$, the first two bands show a clear MLCT character, which disappears upon oxidation, leading to LMCT and MC transitions. This observation is consistent with the drastic decrease in β_{HRS} from $\mathbf{2}^{II}$ to $\mathbf{2}^{III}$ as calculated at the TDDFT level, as well as with the analysis from the VB-CT model (due to the decrease in q_{CT} and d_{CT}). Now, it is interesting to analyze the corresponding behavior in **3**−**5**, which combine the **1** and **2** moieties.

The simulated absorption spectra of both oxidation states of cations **3**−**5** are shown in Figure 7. For the reduced forms, the spectra displays three maxima: around 285, 260, and 210 nm. While their positions remain mostly unaffected (the corresponding ES are slightly red-shifted) upon addition of Ru-bearing moieties ($\mathbf{3}^{II} \rightarrow \mathbf{5}^{II}$), the intensity of the first and last increases, mostly due to the addition of extra ES (the oscillator strengths of the corresponding transitions remain similar). The analysis of the difference in the density of the important ES (Tables S5−S7 and Figures 8−10) shows that the first peak consists of MLCT transitions as expected (like ES #1 of $\mathbf{2}^{II}$, but red-shifted because the π-conjugated path is more important), while the two others have an ILCT character close to that of **1b**. With regard to the oxidized forms, the changes are comparable to the oxidation of **2**: the MLCT character is lost in favor of ILCT, together with an inversion of the displacement of the electron density upon excitation (Tables S8−S10 and Figures 8−10). Note that there are many transitions with weak oscillator strengths, so that only the first peak of $\mathbf{5}^{III}$ (at 268 nm) is obtained when including the first 100 excited states.

Table 4. Nature of the Main Electron Transitions (vertical excitation energy and oscillator strength in parentheses) and Electron Density Difference (negative in blue, isovalue of 0.001 au, two orientations) Together with the Related Quantities [charge transfer amplitude (q_{CT}), distance (d_{CT}), and radius (r_{CT})] of Both Oxidation States of Cation 2 as Computed at the LC-BLYP/6-311G(d)/LANL2TZ Level in Acetonitrile (IEF-PCM)[a]

$\mathbf{2}^{II}$	$\mathbf{2}^{III}$
ES #1, 251 nm (0.237)	ES #1, 239 nm (0.048), $\Delta\langle S^2\rangle = 0.35$
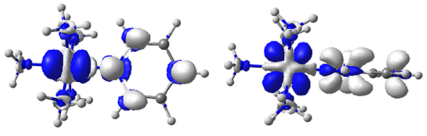	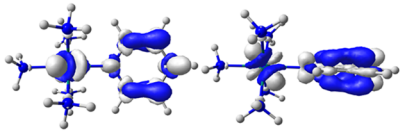
$q_{CT} = 1.00\,e$, $d_{CT} = 2.16$ Å $r_{CT} = -1.71$ Å	$q_{CT} = 0.71\,e$, $d_{CT} = 1.05$ Å $r_{CT} = 1.10$ Å
ES #2, 201 nm (0.155)	ES #2, 228 nm (0.051), $\Delta\langle S^2\rangle = 0.20$
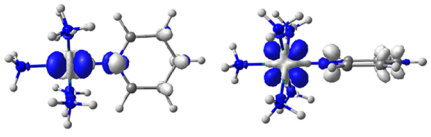	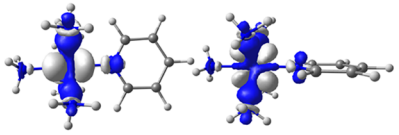
$q_{CT} = 0.65\,e$, $d_{CT} = 2.26$ Å $r_{CT} = -1.72$ Å	$q_{CT} = 0.74\,e$, $d_{CT} = 0.28$ Å $r_{CT} = 0.13$ Å
	ES #3, 206 nm (0.097), $\Delta\langle S^2\rangle = 0.16$
	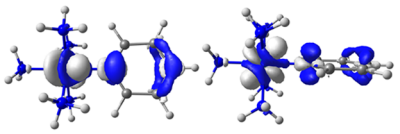
	$q_{CT} = 0.75\,e$, $d_{CT} = 1.81$ Å $r_{CT} = 1.37$ Å

[a]Two molecular orientations are proposed for each transition state.

https://doi.org/10.1021/acs.inorgchem.1c03077
Inorg. Chem. XXXX, XXX, XXX−XXX

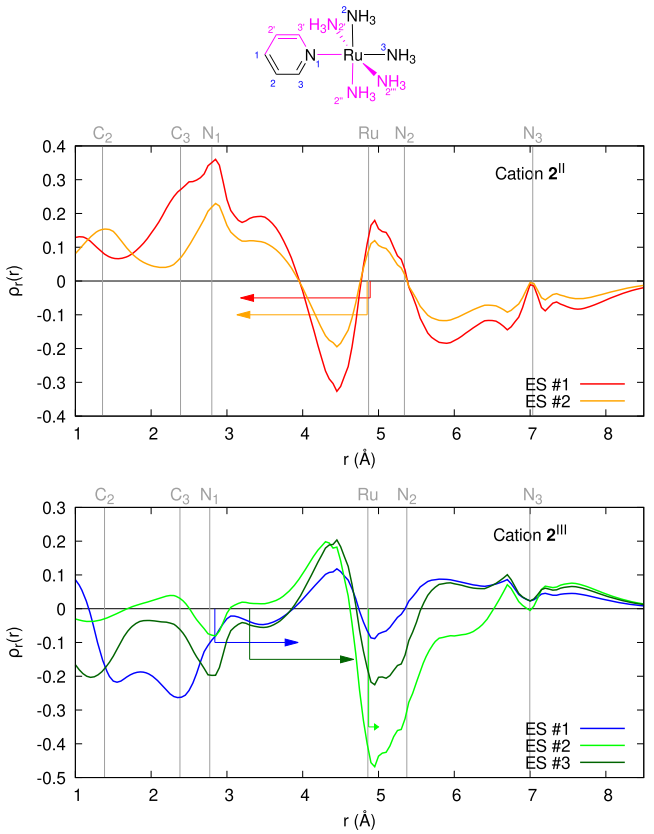

Figure 6. Radial distribution of the electron density difference (centered on the C_1 atom) of the first important excited states of $\mathbf{2}^{\mathbf{II}}$ (middle, numbering of the atoms on top; the purple atoms are equivalent by symmetry) and $\mathbf{2}^{\mathbf{III}}$ (bottom) as computed at the LC-BLYP/6-311G(d)/LANL2TZ level in acetonitrile (IEF-PCM). Arrows indicate $r_{CT} = \langle r \rangle^{+} - \langle r \rangle^{-}$.

4. CONCLUSIONS AND OUTLOOK

In this paper, (time-dependent) density functional theory calculations are enacted to study an octupolar molecular switch bearing six Ru centers, associated with three bidentate ligands forming complexes with the central Zn atom. This switch can be triggered by redox, corresponding to the Ru(II)-to-Ru(III) transformations, and vice versa. The linear and second-order nonlinear optical properties of this challenging complex cation have been studied in its fully reduced and fully oxidized forms. The first hyperpolarizability of the reduced form is 3−4 times larger than that of the oxidized form, as a result of substantial contributions from low-energy metal (Ru)-to-ligand charge

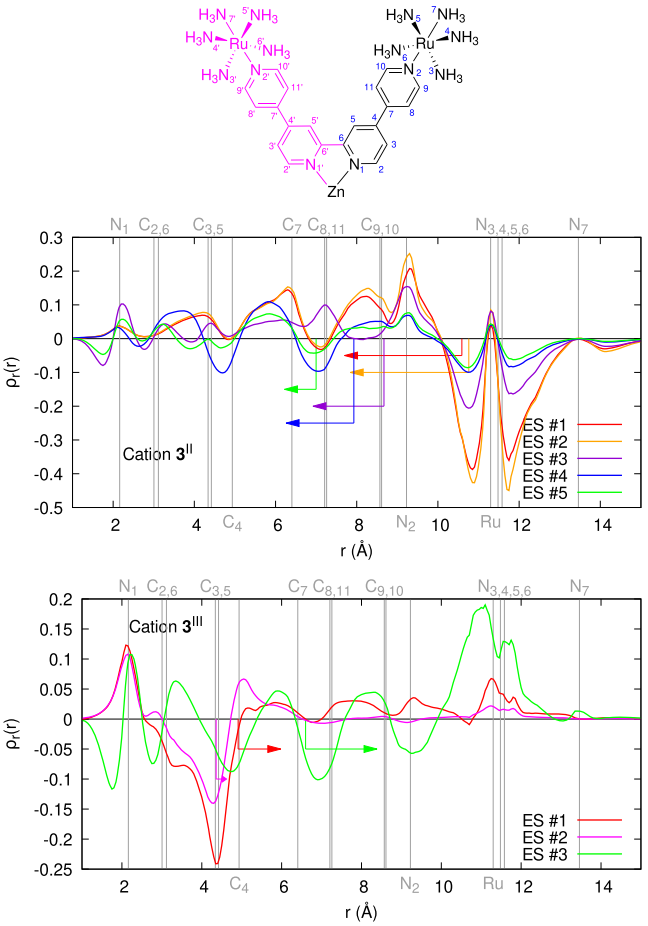

Figure 8. Radial distribution of the electron density difference (centered in Zn) of the first important excited states of $\mathbf{3}^{\mathbf{II}}$ (middle, numbering of the atoms on top; the purple atoms are equivalent by symmetry) and $\mathbf{3}^{\mathbf{III}}$ (bottom) as computed at the LC-BLYP/6-311G(d)/LANL2TZ level in acetonitrile (IEF-PCM). Arrows indicate r_{CT}.

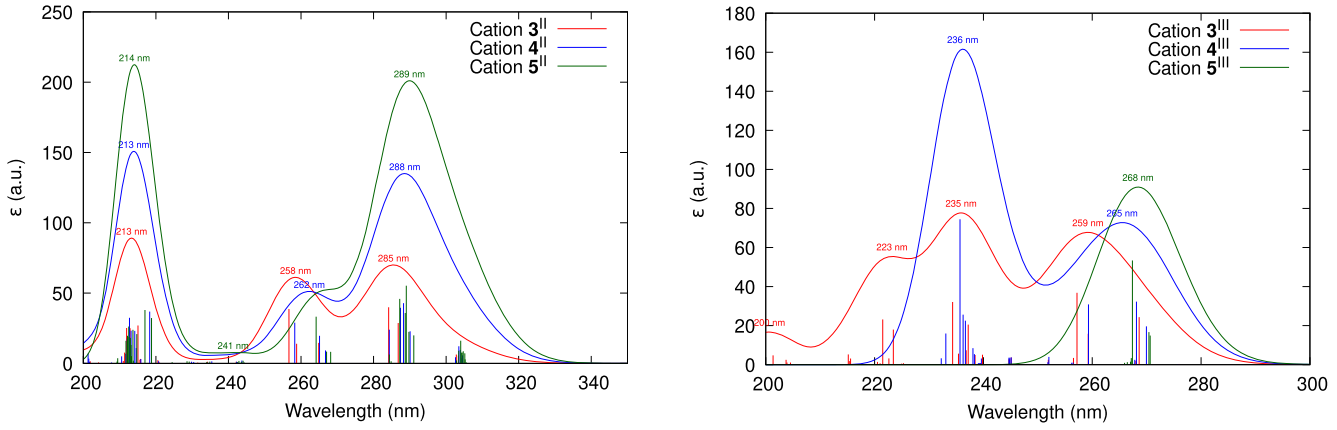

Figure 7. Simulated UV/vis absorption spectra of cations $\mathbf{3}^{\mathbf{II}}$−$\mathbf{5}^{\mathbf{II}}$ (top) and $\mathbf{3}^{\mathbf{III}}$−$\mathbf{5}^{\mathbf{III}}$, as computed at the LC-BLYP/6-311G(d)/LANL2TZ level in acetonitrile (IEF-PCM). Each transition is represented by a Gaussian function (full width at half-maximum of 0.3 eV), together with its impulse. The different maxima of the curves are also reported.

https://doi.org/10.1021/acs.inorgchem.1c03077
Inorg. Chem. XXXX, XXX, XXX−XXX

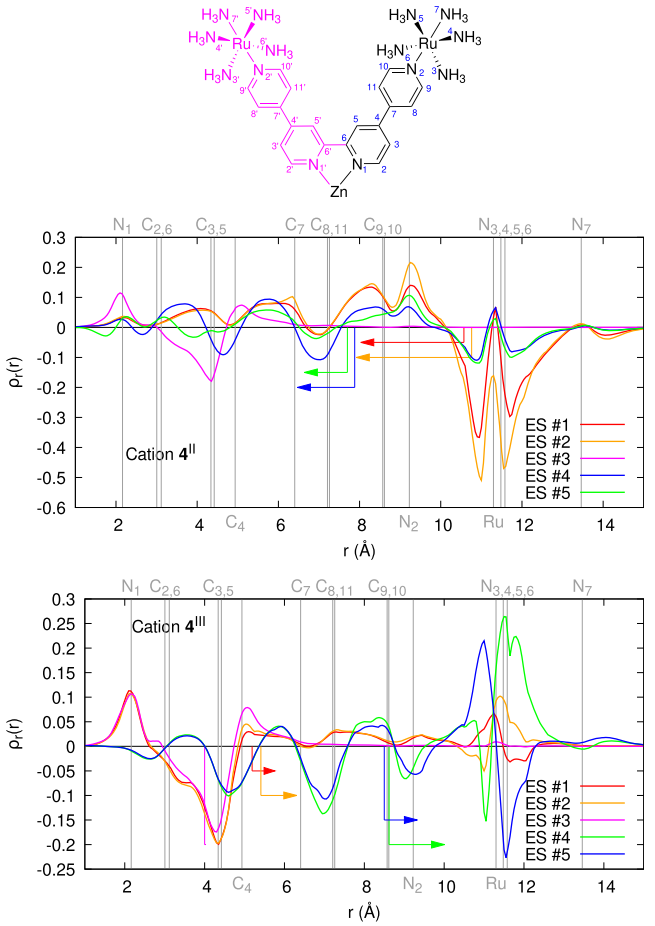

Figure 9. Radial distribution of the electron density difference (centered on the Zn atom) of the first important excited states of $\mathbf{4}^{II}$ (middle, numbering of the atoms on top; the purple atoms are equivalent by symmetry) and $\mathbf{4}^{III}$ (bottom) as computed at the LC-BLYP/6-311G(d)/LANL2TZ level in acetonitrile (IEF-PCM). Arrows indicate r_{CT}. Note that for ES #3 of $\mathbf{4}^{III}$, r_{CT} = 0.02 Å, which is too small to be displayed.

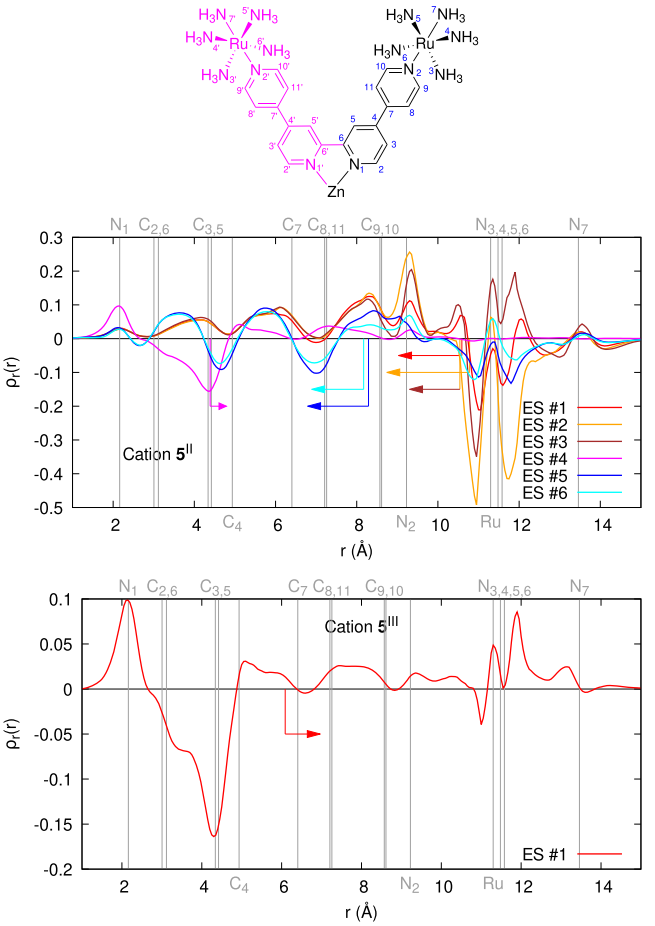

Figure 10. Radial distribution of the electron density difference (centered on the Zn atom) of the first important excited states of $\mathbf{5}^{II}$ (middle, numbering of the atoms on top; the purple atoms are equivalent by symmetry) and $\mathbf{5}^{III}$ (bottom) as computed at the LC-BLYP/6-311G(d)/LANL2TZ level in acetonitrile (IEF-PCM). Arrows indicate r_{CT}.

transfer excited states. On the contrary, upon oxidation, there is a reversal of the direction of charge transfer and a reduction of its amplitude, which explains its smaller first hyperpolarizability. These modifications of the electronic and optical properties upon oxidation have been shown to be associated with a decrease in the level of π-conjugation via a weakening of back bonding between the Ru atoms and the pyridyl ligands, which is evidenced by comparing the ground state geometries.

The first hyperpolarizability of both oxidation states of this octupolar molecular switch has been further analyzed by studying its fragments, in particular those structures obtained by removing one or two bridging ligands. Upon removal of one ligand, the switch contains four Ru centers and corresponds to a Λ-shaped NLOphore, while after removal of two of such ligands, the structure resembles a one-dimensional push−pull NLOphore. For these Λ-shaped and one-dimensional-like systems, the calculations predict, for the reduced form, an enhancement of the first hyperpolarizability by a factor of ∼3. These results have been rationalized by adopting the VB-*n*CT models. Subsequently, this model is used to propose design rules to enhance the first hyperpolarizability of such cations with multiple Ru centers. In particular, in the case of the octupolar structures, it appears to be important to achieve greater charge transfer character in the ground state to enhance the first hyperpolarizability.

In addition to unraveling structure/symmetry−property relationships, this paper has discussed the choice of an appropriate density functional theory level of calculations, by probing the effects of the exchange-correlation functional and of the atomic basis set on the structural and nonlinear optical properties. Finally, the few-state model analysis has been facilitated by adapting to systems having a "radial" structure the method for analyzing the ground-to-excited state electron density differences.

■ ASSOCIATED CONTENT

Supporting Information

The Supporting Information is available free of charge at https://pubs.acs.org/doi/10.1021/acs.inorgchem.1c03077.

Impact of the basis set and XC functional on the geometry of **2**, impact of the basis set and XC functional on the static first hyperpolarizability of **2**, analysis of additional excited states of **1b**, and analysis of excited states of **3**−**5** (PDF)

https://doi.org/10.1021/acs.inorgchem.1c03077
Inorg. Chem. XXXX, XXX, XXX−XXX

AUTHOR INFORMATION

Corresponding Author

Benoît Champagne − *Laboratory of Theoretical Chemistry, Unit of Theoretical and Structural Physical Chemistry, NISM (Namur Institute of Structured Matter), University of Namur, B-5000 Namur, Belgium;* orcid.org/0000-0003-3678-8875; Email: benoit.champagne@unamur.be

Author

Pierre Beaujean − *Laboratory of Theoretical Chemistry, Unit of Theoretical and Structural Physical Chemistry, NISM (Namur Institute of Structured Matter), University of Namur, B-5000 Namur, Belgium;* orcid.org/0000-0003-3723-3257

Complete contact information is available at: https://pubs.acs.org/10.1021/acs.inorgchem.1c03077

Notes

The authors declare no competing financial interest.

ACKNOWLEDGMENTS

The authors thanks Dr. Benjamin J. Coe for having raised this challenge of applying computational chemistry methods to such a complex octupolar system and for his comments. The calculations were performed on the computers of the Consortium des Équipements de Calcul Intensif, including those of the Technological Platform of High-Performance Computing, for which we gratefully acknowledge the financial support of the FNRS-FRFC, of the Walloon Region, and of the University of Namur (Conventions 2.5020.11, GEQ U.G006.15, 1610468, and RW/GEQ2016).

REFERENCES

(1) Coe, B. J. Molecular Materials Possessing Switchable Quadratic Nonlinear Optical Properties. *Chem. - Eur. J.* **1999**, *5*, 2464−2471.

(2) Delaire, J. A.; Nakatani, K. Linear and Nonlinear Optical Properties of Photochromic Molecules and Materials. *Chem. Rev.* **2000**, *100*, 1817−1846.

(3) Nalwa, H. S., Ed. *Handbook of Advanced Electronic and Photonic Materials and Devices*; Academic Press: San Diego, 2001.

(4) Bouas-Laurent, H.; Dürr, H. *Photochromism*; Elsevier, 2003; pp XXVII−LIII DOI: 10.1016/B978-044451322-9/50004-X.

(5) Castet, F.; Rodriguez, V.; Pozzo, J.-L.; Ducasse, L.; Plaquet, A.; Champagne, B. Design and Characterization of Molecular Nonlinear Optical Switches. *Acc. Chem. Res.* **2013**, *46*, 2656−2665.

(6) Clays, K.; Persoons, A. Hyper- Rayleigh Scattering in Solution. *Phys. Rev. Lett.* **1991**, *66*, 2980−2983.

(7) Hendrickx, E.; Clays, K.; Persoons, A. Hyper-Rayleigh Scattering in Isotropic Solution. *Acc. Chem. Res.* **1998**, *31*, 675−683.

(8) Verbiest, T.; Clays, K.; Rodriguez, V. *Second-Order Nonlinear Optical Characterization Techniques: An Introduction*; Taylor & Francis, 2009.

(9) Bublitz, G. U.; Boxer, S. G. Stark Spectroscopy: Applications in Chemistry, Biology, and Materials Science. *Annu. Rev. Phys. Chem.* **1997**, *48*, 213−242.

(10) Finn, R. S.; Ward, J. F. Dc- Induced Optical Second - Harmonic Generation in the Inert Gases. *Phys. Rev. Lett.* **1971**, *26*, 285−289.

(11) Shelton, D. P.; Rice, J. E. Measurements and Calculations of the Hyperpolarizabilities of Atoms and Small Molecules in the Gas Phase. *Chem. Rev.* **1994**, *94*, 3−29.

(12) Kanis, D. R.; Ratner, M. A.; Marks, T. J. Design and Construction of Molecular Assemblies with Large Second-Order Optical Nonlinearities. Quantum Chemical Aspects. *Chem. Rev.* **1994**, *94*, 195−242.

(13) Papadopoulos, M. G.; Sadlej, A. J.; Leszczynski, J. In *Non-Linear Optical Properties of Matter: From Molecules to Condensed Phases*; Papadopoulos, M. G., Sadlej, A. J., Leszczynski, J., Eds.; Challenges and Advances in Computational Chemistry and Physics 1; Springer: Dordrecht, The Netherlands, 2006.

(14) Champagne, B.; Beaujean, P.; de Wergifosse, M.; Cardenuto, M. H.; Liégeois, V.; Castet, F. In *Frontiers of Quantum Chemistry*; Wójcik, M. J., Nakatsuji, H., Kirtman, B., Ozaki, Y., Eds.; Springer: Singapore, 2018; pp 117−138 DOI: 10.1007/978-981-10-5651-2_6.

(15) Bourhill, G.; Brédas, J.-L.; Cheng, L.-T.; Marder, S. R.; Meyers, F.; Perry, J. W.; Tiemann, B. G. Experimental Demonstration of the Dependence of the First Hyperpolarizability of Donor - Acceptor - Substituted Polyenes on the Ground - State Polarization and Bond Length Alternation. *J. Am. Chem. Soc.* **1994**, *116*, 2619−2620.

(16) Lu, D.; Chen, G.; Goddard, W. A. The Valence-bond Charge-transfer-exciton Model for Predicting Nonlinear Optical Properties (Hyperpolarizabilities and Saturation Length) of Polymeric Materials. *J. Chem. Phys.* **1994**, *101*, 4920−4930.

(17) Lu, D.; Chen, G.; Perry, J. W.; Goddard, W. A. Valence- Bond Charge - Transfer Model for Nonlinear Optical Properties of Charge - Transfer Organic Molecules. *J. Am. Chem. Soc.* **1994**, *116*, 10679−10685.

(18) Barzoukas, M.; Fort, A.; Blanchard-Desce, M. A Two - Form Description of Push - Pull Molecules: Correlations between Structure, Intramolecular Charge Transfer and (Hyper) Polarizabilities. *J. Nonlinear Opt. Phys. Mater.* **1996**, *05*, 757−765.

(19) Barzoukas, M.; Runser, C.; Fort, A.; Blanchard-Desce, M. A Two-State Description of (Hyper) Polarizabilities of Push-Pull Molecules Based on a Two-Form Model. *Chem. Phys. Lett.* **1996**, *257*, 531−537.

(20) Kirtman, B.; Champagne, B.; Bishop, D. M. Electric Field Simulation of Substituents in Donor - Acceptor Polyenes: A Comparison with Ab Initio Predictions for Dipole Moments, Polarizabilities, and Hyperpolarizabilities. *J. Am. Chem. Soc.* **2000**, *122*, 8007−8012.

(21) Coe, B. J. Developing Iron and Ruthenium Complexes for Potential Nonlinear Optical Applications. *Coord. Chem. Rev.* **2013**, *257*, 1438−1458.

(22) Coe, B. J.; Essex-Lopresti, J. P.; Harris, J. A.; Houbrechts, S.; Persoons, A. Ruthenium(Ii) Ammine Centres as Efficient Electron Donor Groups Forquadratic Non-Linear Optics. *Chem. Commun.* **1997**, 1645−1646.

(23) Coe, B. J.; Chamberlain, M. C.; Essex-Lopresti, J. P.; Gaines, S.; Jeffery, J. C.; Houbrechts, S.; Persoons, A. Large Molecular Quadratic Hyperpolarizabilities in Donor/Acceptor - Substituted Trans-Tetraammineruthenium (II) Complexes. *Inorg. Chem.* **1997**, *36*, 3284−3292.

(24) Coe, B. J.; Harris, J. A.; Harrington, L. J.; Jeffery, J. C.; Rees, L. H.; Houbrechts, S.; Persoons, A. Enhancement of Molecular Quadratic Hyperpolarizabilities in Ruthenium (II) 4,4′- Bipyridinium Complexes by N - Phenylation. *Inorg. Chem.* **1998**, *37*, 3391−3399.

(25) Coe, B. J.; Houbrechts, S.; Asselberghs, I.; Persoons, A. Efficient, Reversible Redox - Switching of Molecular First Hyper-polarizabilities in Ruthenium (II) Complexes Possessing Large Quadratic Optical Nonlinearities. *Angew. Chem., Int. Ed.* **1999**, *38*, 366−369.

(26) Coe, B. J.; Harris, J. A.; Brunschwig, B. S.; Garín, J.; Orduna, J.; Coles, S. J.; Hursthouse, M. B. Contrasting Linear and Quadratic Nonlinear Optical Behavior of Dipolar Pyridinium Chromophores with 4-(Dimethylamino)Phenyl or Ruthenium (II) Ammine Electron Donor Groups. *J. Am. Chem. Soc.* **2004**, *126*, 10418−10427.

(27) Coe, B. J. In *Non- Linear Optical Properties of Matter: From Molecules to Condensed Phases*; Papadopoulos, M. G., Sadlej, A. J., Leszczynski, J., Eds.; Challenges and Advances in Computational Chemistry and Physics; Springer: Dordrecht, The Netherlands, 2006; pp 571−608 DOI: 10.1007/1-4020-4850-5_18.

(28) Coe, B. J.; Fielden, J.; Foxon, S. P.; Asselberghs, I.; Clays, K.; Brunschwig, B. S. Two- Dimensional, Pyrazine - Based Nonlinear

Optical Chromophores with Ruthenium (II) Ammine Electron Donors. *Inorg. Chem.* **2010**, *49*, 10718−10726.
(29) Coe, B. J.; Pilkington, R. A. Theoretical Studies on Two - Dimensional Nonlinear Optical Chromophores with Pyrazinyl Cores and Organic or Ruthenium (II) Ammine Electron Donors. *J. Phys. Chem. A* **2014**, *118*, 2253−2268.
(30) Zhang, L.-T.; Ondrechen, M. J. The Electronic Structure of Pentaammine (Pyrazine) Ruthenium (II) and (III): The Metal-Ligand π Conjugation and Its Implications in Electron Delocalization. *Inorg. Chim. Acta* **1994**, *226*, 43−51.
(31) Coe, B. J.; Beljonne, D.; Vogel, H.; Garín, J.; Orduna, J. Theoretical Analyses of the Effects on the Linear and Quadratic Nonlinear Optical Properties of N - Arylation of Pyridinium Groups in Stilbazolium Dyes. *J. Phys. Chem. A* **2005**, *109*, 10052−10057.
(32) Escudero, D.; González, L. RASPT2/RASSCF vs Range - Separated/Hybrid DFT Methods: Assessing the Excited States of a Ru (II)Bipyridyl Complex. *J. Chem. Theory Comput.h* **2012**, *8*, 203−213.
(33) Coe, B. J.; Avramopoulos, A.; Papadopoulos, M. G.; Pierloot, K.; Vancoillie, S.; Reis, H. Theoretical Modelling of Photoswitching of Hyperpolarisabilities in Ruthenium Complexes. *Chem. - Eur. J.* **2013**, *19*, 15955−15963.
(34) Zhang, Y.; Castet, F.; Champagne, B. Theoretical Investigation of the First Hyperpolarizability Redox-Switching in a Ruthenium Complex. *Chem. Phys. Lett.* **2013**, *574*, 42−46.
(35) Zhang, Y.; Champagne, B. Understanding the Second - Order Nonlinear Optical Properties of One - Dimensional Ruthenium (II) Ammine Complexes. *J. Phys. Chem. C* **2013**, *117*, 1833−1848.
(36) Escudero, D.; Thiel, W. Assessing the Density Functional Theory-Based Multireference Configuration Interaction (DFT/MRCI) Method for Transition Metal Complexes. *J. Chem. Phys.* **2014**, *140*, 194105.
(37) Escudero, D.; Thiel, W.; Champagne, B. Spectroscopic and Second-Order Nonlinear Optical Properties of Ruthenium (II) Complexes: A DFT/MRCI and ADC (2) Study. *Phys. Chem. Chem. Phys.* **2015**, *17*, 18908−18912.
(38) Zyss, J. Molecular Engineering Implications of Rotational Invariance in Quadratic Nonlinear Optics: From Dipolar to Octupolar Molecules and Materials. *J. Chem. Phys.* **1993**, *98*, 6583−6599.
(39) Cho, M.; Kim, H.-S.; Jeon, S.-J. An Elementary Description of Nonlinear Optical Properties of Octupolar Molecules: Four -State Model for Guanidinium-Type Molecules. *J. Chem. Phys.* **1998**, *108*, 7114−7120.
(40) Coe, B. J. Private communication.
(41) Bersohn, R.; Pao, Y.-H.; Frisch, H. L. Double- Quantum Light Scattering by Molecules. *J. Chem. Phys.* **1966**, *45*, 3184−3198.
(42) Andrews, D. L.; Allcock, P. *Optical Harmonics in Molecular Systems*; Wiley-VCH: Weinheim, Germany, 2002; OCLC: ocm48468465.
(43) Beaujean, P.; Champagne, B. Coupled Cluster Evaluation of the Second and Third Harmonic Scattering Responses of Small Molecules. *Theor. Chem. Acc.* **2018**, *137*, 50.
(44) Frisch, M. J.; et al. *Gaussian 16*, rev. A.03; Gaussian Inc.: Wallingford, CT, 2016.
(45) Groom, C. R.; Bruno, I. J.; Lightfoot, M. P.; Ward, S. C. The Cambridge Structural Database. *Acta Crystallogr. B* **2016**, *72*, 171−179.
(46) Shin, Y.-g. K.; Szalda, D. J.; Brunschwig, B. S.; Creutz, C.; Sutin, N. Electronic and Molecular Structures of Pentaammineruthenium Pyridine and Benzonitrile Complexes as a Function of Oxidation State. *Inorg. Chem.* **1997**, *36*, 3190−3197.
(47) Perdew, J. P.; Wang, Y. Accurate and Simple Analytic Representation of the Electron-Gas Correlation Energy. *Phys. Rev. B* **1992**, *45*, 13244−13249.
(48) Hay, P. J.; Wadt, W. R. Ab Initio Effective Core Potentials for Molecular Calculations. Potentials for K to Au Including the Outermost Core Orbitals. *J. Chem. Phys.* **1985**, *82*, 299−310.
(49) Roy, L. E.; Hay, P. J.; Martin, R. L. Revised Basis Sets for the LANL Effective Core Potentials. *J. Chem. Theory Comput.* **2008**, *4*, 1029−1031.
(50) Colwell, S. M.; Murray, C. W.; Handy, N. C.; Amos, R. D. The Determination of Hyperpolarisabilities Using Density Functional Theory. *Chem. Phys. Lett.* **1993**, *210*, 261−268.
(51) Lee, A. M.; Colwell, S. M. The Determination of Hyperpolarizabilities Using Density Functional Theory with Nonlocal Functionals. *J. Chem. Phys.* **1994**, *101*, 9704−9709.
(52) van Gisbergen, S. J. A.; Snijders, J. G.; Baerends, E. J. Accurate Density Functional Calculations on Frequency-Dependent Hyperpolarizabilities of Small Molecules. *J. Chem. Phys.* **1998**, *109*, 10657−10668.
(53) Ehlers, A. W.; Böhme, M.; Dapprich, S.; Gobbi, A.; Höllwarth, A.; Jonas, V.; Köhler, K. F.; Stegmann, R.; Veldkamp, A.; Frenking, G. A Set of F-Polarization Functions for Pseudo-Potential Basis Sets of the Transition Metals Sc Cu, Y Ag and La Au. *Chem. Phys. Lett.* **1993**, *208*, 111−114.
(54) Richardson, L. F.; Gaunt, J. A. The Deferred Approach to the Limit. Part I. Single Lattice. Part II. Interpenetrating Lattices. *Philos. Trans. R. Soc. London A* **1927**, *226*, 299−361.
(55) Bloor, J. E. Finite Field Ab Initio Calculations of the Dipole Polarizabilities and First and Second Hyperpolarizabilities Using Multiple Sets of Polarization Funct. *Comput. Theor. Chem.* **1991**, *234*, 173−183.
(56) Mohammed, A. A. K.; Limacher, P. A.; Champagne, B. Finding Optimal Finite Field Strengths Allowing for a Maximum of Precision in the Calculation of Polarizabilities and Hyperpolarizabilities. *J. Comput. Chem.* **2013**, *34*, 1497−1507.
(57) de Wergifosse, M.; Liégeois, V.; Champagne, B. Evaluation of the Molecular Static and Dynamic First Hyperpolarizabilities. *Int. J. Quantum Chem.* **2014**, *114*, 900−910.
(58) Iikura, H.; Tsuneda, T.; Yanai, T.; Hirao, K. A Long-Range Correction Scheme for Generalized-Gradient-Approximation Exchange Functionals. *J. Chem. Phys.* **2001**, *115*, 3540−3544.
(59) Cammi, R.; Cossi, M.; Mennucci, B.; Tomasi, J. Analytical Hartree−Fock Calculation of the Dynamical Polarizabilities α, β, and γ of Molecules in Solution. *J. Chem. Phys.* **1996**, *105*, 10556−10564.
(60) Tomasi, J.; Mennucci, B.; Cancès, E. The IEF Version of the PCM Solvation Method: An Overview of a New Method Addressed to Study Molecular Solutes at the QM Ab Initio Level. *Comput. Theor. Chem.* **1999**, *464*, 211−226.
(61) Corozzi, A.; Mennucci, B.; Cammi, R.; Tomasi, J. Structure versus Solvent Effects on Nonlinear Optical Properties of Push - Pull Systems: A Quantum - Mechanical Study Based on a Polarizable Continuum Model. *J. Phys. Chem. A* **2009**, *113*, 14774−14784.
(62) Jacquemin, D.; Bahers, T. L.; Adamo, C.; Ciofini, I. What Is the "Best" Atomic Charge Model to Describe through-Space Charge-Transfer Excitations? *Phys. Chem. Chem. Phys.* **2012**, *14*, 5383.
(63) Campetella, M.; Perfetto, A.; Ciofini, I. Quantifying Partial Hole-Particle Distance at the Excited State: A Revised Version of the DCT Index. *Chem. Phys. Lett.* **2019**, *714*, 81−86.
(64) Huet, L.; Perfetto, A.; Muniz-Miranda, F.; Campetella, M.; Adamo, C.; Ciofini, I. General Density - Based Index to Analyze Charge Transfer Phenomena: From Models to Butterfly Molecules. *J. Chem. Theory Comput.* **2020**, *16*, 4543−4553.
(65) Yang, M.; Champagne, B. Large Off - Diagonal Contribution to the Second - Order Optical Nonlinearities of Λ- Shaped Molecules. *J. Phys. Chem. A* **2003**, *107*, 3942−3951.
(66) Blanchard-Desce, M.; Barzoukas, M. Two-Form Two-State Analysis of Polarizabilities of Push Pull Molecules. *J. Opt. Soc. Am. B* **1998**, *15*, 302.
(67) Cho, M.; An, S.-Y.; Lee, H.; Ledoux, I.; Zyss, J. Nonlinear Optical Properties of Tetrahedral Donor- Acceptor Octupolar Molecules: Effective Five-State Model Approach. *J. Chem. Phys.* **2002**, *116*, 9165−9173.
(68) Orr, B.; Ward, J. Perturbation Theory of the Non-Linear Optical Polarization of an Isolated System. *Mol. Phys.* **1971**, *20*, 513−526.

https://doi.org/10.1021/acs.inorgchem.1c03077
Inorg. Chem. XXXX, XXX, XXX−XXX

(69) Ipatov, A.; Cordova, F.; Doriol, L. J.; Casida, M. E. Excited-State Spin-Contamination in Time-Dependent Density-Functional Theory for Molecules with Open-Shell Ground States. *Comput. Theor. Chem.* **2009**, *914*, 60−73.
(70) Myneni, H.; Casida, M. E. On the Calculation of $\Delta\langle S^2\rangle$ for Electronic Excitations in Time-Dependent Density-Functional Theory. *Comput. Phys. Commun.* **2017**, *213*, 72−91.
(71) Coe, B. J.; Foxon, S. P.; Pilkington, R. A.; Sánchez, S.; Whittaker, D.; Clays, K.; van Steerteghem, N.; Brunschwig, B. S. Rhenium(I) Tricarbonyl Complexes with Peripheral N - Coordination Sites: A Foundation for Heterotrimetallic Nonlinear Optical Chromophores. *Organometallics* **2016**, *35*, 3014−3024.

https://doi.org/10.1021/acs.inorgchem.1c03077
Inorg. Chem. XXXX, XXX, XXX−XXX